Prospects for Detecting Supernova Neutrino Flavor Oscillations

George M. Fuller,[1] and Wick C. Haxton,[2] and Gail C. McLaughlin[2*]
[1] *Department of Physics, University of California, San Diego, La Jolla, CA, 92093-0319*
[2] *Institute for Nuclear Theory, Box 351550, and Department of Physics, Box 351560, University of Washington, Seattle, WA 98195, USA*
(February 1, 2008)

Abstract

The neutrinos from a Type II supernova provide perhaps our best opportunity to probe cosmologically interesting muon and/or tauon neutrino masses. This is because matter enhanced neutrino oscillations can lead to an anomalously hot ν_e spectrum, and thus to enhanced charged current cross sections in terrestrial detectors. Two recently proposed supernova neutrino observatories, OMNIS and LAND, will detect neutrons spalled from target nuclei by neutral and charged current neutrino interactions. As this signal is not flavor specific, it is not immediately clear whether a convincing neutrino oscillation signal can be extracted from such experiments. To address this issue we examine the responses of a series of possible light and heavy mass targets, ^{9}Be, ^{23}Na, ^{35}Cl, and ^{208}Pb. We find that strategies for detecting oscillations which use only neutron count rates are problematic at best, even if cross sections are determined by ancillary experiments. Plausible uncertainties in supernova neutrino spectra tend to obscure rate enhancements due to oscillations. However, in the case of ^{208}Pb, a signal emerges that is largely flavor specific and extraordinarily sensitive to the ν_e temperature, the emission of two neutrons. This signal and its flavor specificity are associated with the strength and location of the first-forbidden responses for neutral and charge current reactions, aspects of the ^{208}Pb neutrino cross section that have not been discussed previously. Hadronic spin transfer experiments might be helpful in confirming some of the nuclear structure physics underlying our conclusions.

14.60.Pq, 26.50.+x, 25.30.Pt

*Current Address: TRIUMF, 4004 Wesbrook Mall, Vancouver, B.C. Canada V6T2A3. Electronic address: gail@alph01.triumf.ca

I. INTRODUCTION

In this paper we investigate some of the difficulties in detecting the effects of neutrino flavor oscillations on the neutrino spectra from Type II supernovae. In particular, we examine what might be learned from different target materials in proposed, long-duration neutrino experiments such as the Observatory for Multiflavor Neutrinos from Supernovae (OMNIS [1,2]) and the Lead Astronomical Neutrino Detector (LAND [3]). These detectors would record neutrons spalled from nuclei following inelastic neutrino excitations. While neutrons can be produced in either neutral or charge current interactions, the relative strength of these two contributions is sensitive to target thresholds and charge, and thus can be adjusted through the choice of target material.

In this way sensitivity to neutrino flavor can be achieved. For example, one expects a target with low Z and a high charged-current threshold to be characterized by a low (ν_e,e$^-$) cross section, and thus to produce neutrons primarily through neutral current interactions, particularly if the target is also characterized by a low neutron separation threshold. Alternatively, a target with a high Z, so that Coulomb effects enhance the phase space for emitted electrons, and low (ν_e,e$^-$) threshold should have a much stronger response to charge current interactions. The main purpose of this study is to explore what can be achieved with such target strategies, taking into account the considerable uncertainties that exist in our understanding of supernova ν_e, $\bar{\nu}_e$ and heavy-flavor neutrino spectra.

An observation of neutrino flavor transformation, or the demonstration that this phenomena does not occur over some range of neutrino masses and mixing angles, would have important consequences for both particle physics and astrophysics (for a review see Ref. [4]). Neutrino flavor oscillations arise in extended models in which neutrinos are massive or have magnetic moments, and in which the flavor and mass eigenstates are not coincident. The strength of the flavor mixing can be greatly enhanced in matter, with two familiar examples being spin-flavor precession [5] and the Mikheyev-Smirnov-Wolfenstein (MSW) [6] mechanism, with the latter being the most popular proposed solution of the solar neutrino problem.

The deficit of solar neutrinos relative to the predictions of the standard solar model can be explained by $\nu_e \rightarrow \nu_\mu$ or $\nu_e \rightarrow \nu_\tau$ flavor oscillations (or by an oscillation to a sterile state $\nu_e \rightarrow \nu_s$). The favored MSW solution for the sun suggests that the mass-squared difference between ν_e and the second neutrino involved in the oscillation is $\delta \mathrm{m}^2 \sim 10^{-5}$ eV. If this second neutrino is the ν_μ, then the seesaw mechanism [8] predicts a mass hierarchy where the ν_μ mass $\sim$ few $\times 10^{-3}$ eV and the ν_τ mass is in or near the cosmologically interesting range, 1 to 100 eV [9]. This is an attractive scenario as it allows the ν_τ to be a source of hot dark matter.

If neutrino oscillations are responsible for the solar neutrino problem, similar effects should arise for supernova neutrinos. Very general arguments lead to a hierarchy of average energies for supernova neutrinos, $\langle E_{\nu_\tau} \rangle \sim \langle E_{\bar{\nu}_\tau} \rangle \sim \langle E_{\nu_\mu} \rangle \sim \langle E_{\bar{\nu}_\mu} \rangle > \langle E_{\bar{\nu}_e} \rangle > \langle E_{\nu_e} \rangle$. This pattern is established near the neutrinosphere (roughly the surface of the neutron star), where the neutrinos decouple from the matter at a density of $\sim 10^{12}$ g cm^{-3}.

Neutrino oscillations can alter this pattern in a distinctive way, producing a characteristic signature in terrestrial supernova detectors, given an MSW neutrino mass level crossing outside the neutrinosphere. As the density at the neutrinosphere is 10 orders of magnitude

greater than that of the solar core, such crossings occur for an extended range of $\delta m^2 = m_H^2 - m_L^2$, where m_H and m_L are the masses of the heavy and light neutrino eigenstates being mixed. The resulting values, 10^{-5} eV$^2 \leq \delta$ m$^2 \leq 10^6$ eV^2, encompasses not only the MSW solutions discussed in connection with the solar neutrino problem, but also mixing that might be associated with cosmologically interesting tauon neutrino masses.

Neutrino flavor transformation can also have important consequences for supernova dynamics and nucleosynthesis. After collapse and core bounce, the energy spectra of neutrinos emitted from the neutrino sphere of the cooling proto-neutron star are approximately Fermi-Dirac, with small chemical potentials. Although a crude equipartition of energy between neutrino species is imposed by the weak equilibrium that obtains in the core, the subsequent decoupling of the neutrinos from the matter at the neutrinosphere is flavor dependent and leads to the hierarchy of average energies noted above. The ν_μ, $\bar{\nu}_\mu$, ν_τ, and $\bar{\nu}_\tau$ species decouple deepest in the core because they lack charged current reactions with nucleons and have smaller cross sections for scattering off electrons than the ν_e and $\bar{\nu}_e$ species. The ν_es have the lowest average energy because they are the last to decouple: matter near the neutrinosphere is partially deleptonized and thus rich in neutrons, enhancing $\nu_e + \mathrm{n} \rightarrow \mathrm{p} + \mathrm{e}^-$. For example, in one study the ν_μ, $\bar{\nu}_\mu$, ν_τ, and $\bar{\nu}_\tau$ have average energies $\langle E_{\nu_\mu} \rangle \sim 25\,\mathrm{MeV}$, while the electron neutrinos and antineutrinos have energies $\langle E_{\bar{\nu}_e} \rangle \sim 16\,\mathrm{MeV}$ and $\langle E_{\nu_e} \rangle \sim 11\,\mathrm{MeV}$ [10]. Neutrinos may be responsible for the revival of the supernova shock wave, which stalls in most numerical simulations at a radius of around 200 - 400 km above the surface of the protoneutron star shortly after core bounce, $t_{\mathrm{pb}} \sim 0.1$ s. Neutrino interactions in the nucleon gas left in the wake of the shock wave can deposit considerable energy, providing the push needed for a successful explosion. Oscillations can enhance this effect: If a $\nu_e \leftrightarrow \nu_\tau$ oscillation took place between the edge of the neutron star and the stalled shock at this epoch, the resulting more energetic ν_e flux increases the rate of neutrino heating [11]. Neutrino flavor oscillations can also alter supernova nucleosynthesis at later times $t_{\mathrm{pb}} \gtrsim 3\,\mathrm{s}$ [10].

Terrestrial experiments exploiting accelerator or reactor neutrino sources, such as LAMPF's Liquid Scintillator Neutrino Detector (LSND [12]) and the CERN experiments NOMAD [13] and CHORUS [14], are placing constraints on vacuum oscillations. To date, no evidence for $\nu_\mu \leftrightarrow \nu_\tau$ mixing has been found at NOMAD or CHORUS. LSND has attributed an excess of events above background to $\bar{\nu}_\mu \rightarrow \bar{\nu}_e$, although these events have also been interpreted as an upper limit [12]. The KARMEN [15] experiment, which is similar to LSND in its sensitivity to δm^2 and mixing angle, has not yet accumulated enough data to convincingly confirm or rule out the LSND result. But perhaps the strongest indication of oscillations comes from the deficit of muons in the interactions of upward going atmospheric neutrinos, as recently reported by the SuperKamiokande collaboration [16]. The solar neutrino problem, atmospheric neutrino anomaly, and LSND results all suggest new physics, though all of these anomalies together are difficult to reconcile with a simple pattern of neutrino masses and mixing angles arising in theories with only three active neutrinos [17].

Important new constraints on neutrino properties can be extracted from observations of supernova neutrinos. One technique for measuring neutrino mass, independent of mixing angles, exploits the time delay and/or spreading in the neutrino signal (see for example Ref. [2]). The arrival time difference for ν_e and ν_τ neutrinos with masses m_{ν_e} and m_{ν_τ}, respectively, is

$$\delta t \sim 0.514 R_{10\,\mathrm{kpc}} [(m_{\nu_\tau}/E_{\nu_\tau})^2 - (m_{\nu_e}/E_{\nu_e})^2], \tag{1}$$

where E_{ν_τ} and E_{ν_e} are the energies of the tauon and electron neutrinos, $R_{10\,\mathrm{kpc}}$ is the distance to the supernova in 10 kiloparsecs (comparable to the galactic radius), and δt is measured in seconds. (Alternatively, one can rewrite Eq. (1) for a single flavor, but with arrival times dependent on the neutrino energy.) The result is a characteristic spreading of the neutrino pulse, with arrival times correlated with the neutrino energy and/or flavor. Neutrino masses, or limits on masses, can be deduced by comparing an observed neutrino signal with the spectra and time-dependent luminosities arising in plausible supernova models.

Measurements made by Kamiokande and IMB at the time of SN1987A were argued to provide a limit on the $\bar{\nu}_e$ mass. The analysis were limited by the small number of detected neutrino events and by uncertainties in modeling the supernova mechanism and associated neutrino emission [18]. As a result, the deduced limits span a considerable range. Clearly such astrophysical uncertainties will also affect future time-of-flight neutrino mass limits derived from new detectors like OMNIS and LAND. Yet these detectors should have two important advantages. First, they promise a large number of neutrino events for a galactic supernova, possibly giving us a detailed time history of neutrino emission associated with the supernova. For example, it was recently argued that large event rates would allow experimentalists to map out the expected initial sharp rise in neutrino emission following core bounce, a feature in the neutrino cooling curve that could be exploited to significantly tighten mass limits [19]. Second, complimentary information from other new detectors, such as SuperKamiokande [20], will reduce the degree to which analyses must depend on poorly understood aspects of supernova models. The spectrum and flavor of supernova neutrinos will be more accurately characterized given a complement of detectors with different thresholds and flavor sensitivities. Flavor specificity in time-of-flight measurements is quite important because competing laboratory limits on the ν_τ and ν_μ masses, 24 MeV and 170 keV, respectively, are so poor.

If neutrinos mix, supernovae could provide an important consistency check on models of neutrino masses and also possibly on time of flight derived neutrino masses. Flavor oscillations, enhanced by matter effects, can lead to transformation between ν_e's and either the ν_μ or ν_τ, leading to an anomalously energetic ν_e spectrum. This departure from the usual hierarchy of average neutrino energies is a powerful test for new physics because it will occur for an extended range of $\delta\mathrm{m}^2$ and mixing angles. In fact, the neutrino mass level crossings become increasingly adiabatic for larger $\delta\mathrm{m}^2$, with adiabatic flavor transformation occurring for mixing angles $\sin^2\theta \gtrsim 10^{-5}$. Thus the observation of an excess of supernova ν_e events provides an opportunity to probe neutrino phenomena that may be inaccessible otherwise.

Several detectors, both in operation and proposed, could detect neutrinos from a galactic supernova. (A partial review can be found in [21].) Two of particular note are the light water Cerenkov detector SuperKamiokande, which has an inner fiducial volume of 22.5 kilotons and has been in operation for approximately two years; and the Sudbury Neutrino Observatory [22], a heavy water Cerenkov detector whose inner vessel will contain one kiloton of D_2O. SNO is currently in its commissioning phase and should be fully operational by the end of 1998. In SNO charged and neutral current reactions will produce distinct signals. The neutral current neutrino reaction $\mathrm{D}(\nu_\mathrm{x}, \nu'_\mathrm{x})\mathrm{np}$ produces free neutrons. These will be detected either by their (n,γ) reactions on ^{35}Cl, which will be introduced by dissolving salt in the water, or by their interactions in specially designed counters utilizing the ^{3}He(n,p) reaction.

The charged current reaction D(ν_e,e$^-$)pp produces energetic electrons that will be observed through Cerenkov light. (The absence of coincident neutrons distinguishes this reaction from D($\bar{\nu}_e$,e$^+$)nn.) A supernova neutrino burst altered by $\nu_e \leftrightarrow \nu_\mu/\nu_\tau$ oscillations will produce an enhanced (ν_e,e$^-$) signal, while leaving the rest unchanged.

SuperKamiokande is of particular interest because of its size and its likely longevity: the collaboration hopes to operate the detector for three decades, a period approaching the timescale for galactic supernova. However the enormous event rate for ($\bar{\nu}_e$,e$^+$) off free protons tends to obscure, in the case of flavor oscillations, the ν_e signal of interest. Perhaps the best opportunity for measuring the ν_e's is through the reaction ^{16}O(ν_e,e$^-$), which produces a back-angle enhancement in the electron distribution that will distort the known (and nearly isotropic) distribution from ($\bar{\nu}_e$,e$^+$) [23].

In contrast, the flavor oscillation effects on the forward-peaked events from ν-electron scattering are very subtle and difficult to extract. This cross section is approximately linear in the neutrino energy and so there is no net change in the event rate due to flavor oscillations. The event rate is then proportional to the luminosity, which we noted earlier was approximately independent of flavor. Note that this contrasts with semileptonic interactions, where cross sections scale as E_ν^2 or faster, depending on nuclear thresholds. Yet there is a shift in the distribution of forward-peaked events towards higher energy from neutrino-electron scattering. This is because the ν_e-electron cross section is approximately six times that the cross section for heavy flavor neutrinos. In turn, this effect may provide a signal for flavor oscillations [24].

Another interesting possibility, suggested quite recently [25], is the detection of the 5-10 MeV γ rays produced in cascades following the neutral current breakup of ^{16}O. A supernova at a distance of 10 kpc would produce a few hundred such events from ν_μ and ν_τ interactions in SuperKamiokande. A tauon mass could then be extracted from analysis of the time evolution of the signal [26].

One of the arguments for detectors such as OMNIS and LAND is that they could remain in operation over a long period of time, making the probability of observing a galactic supernova reasonably high. These detectors would record neutrons produced in the neutral current breakup of nuclei,

$$\nu_i + (\mathrm{Z,N}) \rightarrow (\mathrm{Z,N-1}) + \nu_i + n, \tag{2}$$

where i represents all neutrino and antineutrino species. Here (Z,N) denotes a nucleus with Z protons and N neutrons. A similar signal can arise for the analogous charged current reactions

$$\nu_e + (\mathrm{Z,N}) \rightarrow (\mathrm{Z+1,N-2}) + e^- + n \tag{3}$$

and

$$\bar{\nu}_e + (\mathrm{Z,N}) \rightarrow (\mathrm{Z-1,N}) + e^+ + n. \tag{4}$$

By itself, the observation of a neutron in OMNIS or LAND provides no information on the type of initiating neutrino reaction. The goals of this paper include calculating the cross sections and spallation probabilities for these detectors more carefully than has been attempted before; exploring to what extent the use of multiple nuclear targets might

enhance flavor sensitivity; and exploring what can be learned by comparing the rates for one and two neutron spallation. Ideally one would hope to find targets with very different relative sensitivities to ν_e and neutral current reactions. The success of such a strategy clearly depends on our ability to accurately calculate (or measure) the neutrino responses of the targets, and to estimate uncertainties in supernova flux predictions.

In section II we discuss neutrino-induced neutron spallation in both high Z and low Z target materials, describing the underlying nuclear structure physics governing the responses. We also provide estimates of cross sections for four possible target materials, ^{9}Be, ^{23}Na, ^{35}Cl and ^{208}Pb. In section III we discuss strategies for determining whether the neutrino flux has been altered by oscillations. Although our study is by no means exhaustive, it appears that the tactic of looking for changes in total spallation cross sections is rather challenging. It is very difficult, even using multiple targets, to achieve the necessary degree of sensitivity to the ν_e temperature. The primary difficultly is our uncertain knowledge of the spectrum of supernova neutrinos in the absence of oscillations. The one exception we found to this general rule is the two neutron spallation channel in ^{208}Pb, which appear to provide an exquisitely sensitive ν_e thermometer. The underlying physics involves the first-forbidden contributions to the charged and neutral current channels which have not been considered previously. We suggest some experimental work that would help in characterizing the ^{208}Pb response to neutrinos.

II. NEUTRINO-NUCLEUS INTERACTIONS

In this section we discuss supernova neutrino reactions with nuclear targets which lead to the spallation of one or more neutrons. There are three main physics issues. The first is estimating the target response: what is the distribution of final nuclear states that will result when target nuclei interact with an incident spectrum of neutrinos? For the relatively low neutrino energies of interest, the nuclear response is dominated by allowed and first-forbidden transitions. Fortunately we have a number of experimental tests of these responses, and there exist approximate sum rules that are both important guides to and constraints on calculations.

The second issue is the probability that a neutrino interaction will result in the emission of a neutron, thus producing a signal in the detector. Neutron emission can only occur if the daughter nucleus is excited above the neutron separation energy. The branching ratio into this channel also depends on the competition with other open channels, such as proton or α emission. We estimate these in Hauser-Feshbach calculations.

The third issue is the supernova neutrino spectrum. Because the threshold for neutron spallation can be substantially, often the high energy tail of the neutrino spectrum is especially important in determining the overall rate. Various numerical simulations of supernova explosions differ in the approximations made in treating neutrino diffusion, convection, etc. Thus, while there is qualitative agreement about the average energy hierarchy discussed in the introduction, there are differences in the precise value of the average energy and in the details of the spectrum shape. The resulting uncertainties clearly have an influence on predictions of flux-averaged nuclear cross sections.

The last of these issues, the neutrino spectrum, enters in evaluating the flux-averaged cross section

$$\langle\sigma\rangle = \int_{E_{th}}^{\infty} f_\nu(E_\nu)\,\sigma(E_\nu)dE_\nu, \tag{5}$$

where E_{th} is the threshold energy for the reaction, f_ν is the normalized neutrino spectrum, and $\sigma(E_\nu)$ is the nuclear cross section for an incident neutrino of energy E_ν. The supernova neutrino energy spectra predicted by transport codes can be represented approximately by modified Fermi-Dirac distributions of the form [27,28]

$$f_\nu = \left[\frac{1}{T_\nu^3 F_2(\eta_{eff})}\right] \frac{E_\nu^2}{\exp(E_\nu/T_\nu - \eta_{eff}) + 1}. \tag{6}$$

Here T_ν and η_{eff} are the neutrino temperature and degeneracy parameter (chemical potential divided by T_ν), respectively, and $F_2(\eta_{eff})$ is the relativistic Fermi integral of order 2 and argument η_{eff}, required to normalize the above distribution to unity. The Fermi integrals of order k are defined by

$$F_k(\eta) \equiv \int_0^\infty \frac{x^k dx}{\exp(x-\eta)+1}. \tag{7}$$

The flux $d\Phi_\nu$ of neutrinos with energies between E_ν and $E_\nu + dE_\nu$ a large distance r from a supernova can then be written

$$d\Phi_\nu(E_\nu) = \frac{L_\nu}{4\pi r^2}\frac{1}{\langle E_\nu\rangle} f(E_\nu)dE_\nu, \tag{8}$$

where L_ν is the luminosity of the neutrino species of interest. Note that $\langle E_\nu\rangle = T_\nu F_3(\eta_{eff})/F_2(\eta_{eff})$ and is $\sim 3.15T_\nu$ when η_{eff}=0 and $\sim 3.99T_\nu$ when $\eta_{eff} = 3$.

Predictions of neutrino energy spectra and luminosities vary between different supernova neutrino transport codes, thus producing different values of η_{eff} and T_ν when approximated as in Eq. (7). For example, the transport calculations by Janka yield spectra with $\eta_{eff} \sim 3$ for all neutrino species [28]. While this choice also produces a good fit to the ν_e and $\bar{\nu}_e$ spectra of Wilson and Mayle [27], their heavy-flavor neutrino spectra more closely resemble a black-body distribution ($\eta_{eff} \sim 0$). Such differences are an important source of uncertainties in predicting neutron counting rates in a detector, a point we will return to in section III.

We now turn to the issue of the neutrino reaction cross sections. At typical supernova neutrino energies one expects the total cross section for the charged current reaction (ν_e,e$^-$) on a parent nucleus of charge Z to be dominated by the allowed transitions to the isobaric analog state (IAS) and the Gamow-Teller (GT) resonance states in the daughter nucleus. The allowed cross section is

$$\sigma(E_{\nu_e}) = \frac{G_F^2\cos^2\theta_c}{\pi} k_e E_e F(Z+1,E_e)[|M_F|^2 + (g_A^{\rm eff})^2|M_{GT}|^2], \tag{9}$$

where G_F is the Fermi constant, E_e and k_e are the energy and three-momentum of the outgoing electron, respectively, θ_c is the Cabibbo angle, and $F(Z+1,E_e)$ accounts for the Coulomb distortion of the outgoing electron wave function, which we take from the tabulations of Behrends and Janecke [29]. In several cases we will study below, the total BGT strength is taken from shell model calculations that satisfy the Ikeda sum rule implicitly

(see below). Phenomenologically it is known that these approaches will overestimate low-lying BGT strength unless an effective axial-vector coupling constant $g_A^{\rm eff} \approx 1$ is used, rather than the bare nucleon value 1.26 [30]. Thus we allow for such a renormalized $g_A^{\rm eff}$.

The allowed Fermi and GT transition strengths are

$$|M_F|^2 = \frac{1}{2J_i+1}|\langle J_f||\sum_{i=1}^{A}\tau_+(i)||J_i\rangle|^2, \tag{10}$$

and

$$|M_{\rm GT}|^2 = \frac{1}{2J_i+1}|\langle J_f||\sum_{i=1}^{A}\sigma(i)\tau_+(i)||J_i\rangle|^2, \tag{11}$$

respectively. To evaluate the cross section one must specify the distribution of these transition probabilities over the final states of the daughter nucleus. All of the formulas above also apply to ($\bar{\nu}_e$,e$^+$) provided the corresponding Coulomb correction $F(Z-1,E_e)$ is evaluated for a positron and the isospin operators are replaced by $\tau_-(i)$.

In the limit of good isospin the Fermi strength $|M_F|^2 = |N-Z|$ is carried entirely by the IAS in the daughter nucleus. All of the nuclei of present interest (^{9}Be, ^{23}Na, ^{35}Cl, ^{208}Pb) are neutron rich, so Fermi transitions contribute only to the (ν_e,e$^-$) direction. The Fermi transitions for the first three nuclei populate the mirror ground states of the daughter nuclei, none of which decays by neutron emission. Thus they are of no interest to us. The analog state in ^{208}Bi, however, is located at an excitation energy of 15.16 MeV, well above the neutron breakup threshold and just barely (0.2 MeV) above the two-neutron breakup threshold. Therefore

$$|M_F(E)|^2 = 44\,\delta_{E\,E'}, \quad {}^{208}{\rm Pb}(\nu_e,e^-)^{208}{\rm Bi} \tag{12}$$

where $E = E_\nu - E_e$ is the nuclear (not atomic) excitation energy measured relative to the parent ground state in ^{208}Pb, and $E' \approx 17.53\,$MeV.

The GT strength is more complex. The difference between the GT strength in the (ν_e,e$^-$) channel and that in the ($\bar{\nu}_e$,e$^+$) direction is governed by the Ikeda sum rule, $\sum_f |M_{\rm GT}|^2 \sim 3(N-Z)$, but this sum rule is generally not saturated by the low-energy GT resonance found in (p,n) studies. Presumably the missing strength is pushed to higher excitation energies, where it would influence low-energy neutrino reactions very little. Thus the relevant issue for us is to determine how much of the sum rule is exhausted by accessible strength. In the case of ^{208}Pb, the naive shell model description (closed proton and neutron major shell at 82 and 126, respectively) predicts that the ($\bar{\nu}_e$,e$^+$) direction is completely blocked. The strength in the (ν_e,e$^-$) direction has been measured by forward-angle (p,n) scattering [31]. Consistent with the general trends of GT strength distributions with N-Z, the centroid of the distribution for this neutron rich nucleus is quite low, just 0.4 MeV above the position of the IAS. The resonance is quite narrow and can be reasonably fit by a Gaussian with a full width at half maximum $\Gamma = 2(\ln 2)^{1/2}\Delta \sim 4$ MeV and with total strength equivalent to above 46% of the Ikeda sum rule [32]. Thus

$$(g_A^{eff})^2|M_{\rm GT}(E)|^2 \sim \frac{96.2}{\Delta\sqrt{\pi}}\exp[-(E-E_{\rm GT})^2/\Delta^2], \quad {}^{208}{\rm Pb}(\nu_e,e^-)^{208}{\rm Bi}, \tag{13}$$

where $E_{GT} \sim 17.9$ MeV and $\Delta \sim 2.4$ MeV. The strength assigned above comes from normalizing the (p,n) cross section to that for the Fermi transition [32], which is probably the most reliable normalization given the paucity of strong GT transitions of known strength among heavier nuclei. However, the "universal scaling" approach, which depends on the (p,n)/β decay proportionality derived primarily from lighter nuclei, would reduce the integrated strength in the ^{208}Bi peak to 64% of the value above [32]. Therefore it is not unreasonable to assign a $\pm$ 50% uncertainty to this GT resonance estimate.

The light nuclei of interest, ^{9}Be, ^{23}Na, and ^{35}Cl, lie in the middle of shells, so consequently both the (ν_e,e$^-$) and ($\bar{\nu}_e$,e$^+$) channels are open. In these cases GT strength distributions are taken from shell model calculations in which all configurations in the $1p$ or $2s1d$ shells, as appropriate, are allowed to interact. This guarantees that the Ikeda sum rule is preserved. The interactions used are Cohen and Kurath [33] and Brown-Wildenthal [34]. These calculations, of course, determine both the integrated GT strength and its distribution. We use $g_A^{eff} \sim 1$ to take into account the empirical discrepancy between the results of such sum-rule-preserving calculations and experimental estimates of quenching in the region of the GT resonance.

In allowed neutral current neutrino scattering, the analog of the Fermi operator only contributes to elastic scattering. Thus inelastic allowed transitions are governed by the neutral current GT transition probability

$$|M_{\rm GT}^{\rm NC}|^2 = \frac{1}{2J_i+1}|\langle J_f||\sum_{i=1}^{A}\sigma(i)\frac{\tau_3(i)}{2}||J_i\rangle|^2. \tag{14}$$

This operator is closely connected to the isovector M1 operator, as the spin contribution to the M1 operator tends to dominate because of the large isovector magnetic moment, $\mu_{\rm V}$ = 4.706. The distribution of M1 strength in ^{208}Pb has been the subject of a great deal of study. Experimental searches for the M1 strength [35,36] and theoretical efforts to identify the quenching effects of correlations [37,38] has led to a reasonably consistent picture of the underlying physics. The simplest closed-shell description attributes the M1 response to proton $(h_{9/2})(h_{11/2})^{-1}$ and neutron $(i_{11/2})(i_{13/2})^{-1}$ particle-hole excitations. The residual interaction mixes these configurations, with the symmetric combination that saturates the isoscalar response centered at an excitation energy of about 5.8 MeV, while the isovector response (the quantity of interest to us) is centered on a resonance straddling the neutron breakup threshold at 7.368 MeV. The quenching, attributed to more complicated multiparticle-hole correlations, reduces the naive isovector B(M1) from $\sim 50\,\mu_N^2$ (nucleon Bohr magnetons squared) to $\sim 20\,\mu_N^2$. Experiment finds $8.8\mu_N^2$ below the neutron breakup threshold, and $6.8\mu_N^2$ immediately above. Theory [37] finds a weak tail of strength at excitation energies between 10 and 20 MeV of about $0.6\mu_N^2$.

The integrated isovector B(M1) strength (in units of μ_N^2) can be related to the neutral current response

$$B(M1) = \frac{3\mu_{\rm V}^2}{4\pi}|M_{\rm GT}^{\rm NC}|^2\eta^2 \tag{15}$$

where

$$\eta = 1 + \frac{\langle J_f||\sum_{i=1}^{A} l(i)\tau_3(i)||J_i\rangle}{\mu_{\rm V}\langle J_f||\sum_{i=1}^{A}\sigma(i)\tau_3(i)||J_i\rangle} \tag{16}$$

We find $\eta = 0.894$ using the simple particle-hole description of the ^{208}Pb isovector M1 resonance (in effect assuming that a ratio of orbital and spin matrix elements will not be greatly changed when correlations responsible for quenching are turned on). The choices $E_{GT} = 7.32$ MeV and $\Delta = 0.6$ MeV yield a reasonable fit to the measured width of the isovector M1 response and the proper straddling of the neutron breakup threshold. So adopting the experimental isovector M1 strength of (8.8+6.8+0.6) μ_N^2, the distribution of allowed strength for neutral current neutrino scattering is obtained,

$$(g_A^{eff})^2 |M_{\rm GT}^{\rm NC}(E)|^2 \sim \frac{6.1}{\Delta\sqrt{\pi}} \exp[-(E - E_{\rm GT})^2/\Delta^2], \quad ^{208}{\rm Pb}(\nu_i, \nu_f)^{208}{\rm Pb}, \tag{17}$$

where $E = E_{\nu_i} - E_{\nu_f}$ is the nuclear excitation energy in ^{208}Pb. Approximately 55% of this distribution lies below neutron breakup threshold and thus does not contribute to the spallation. The corresponding allowed cross section is

$$\sigma(E_{\nu_i}) = \frac{G_F^2}{\pi} E_{\nu_f}^2 (g_A^{\rm eff})^2 |M_{\rm GT}^{\rm NC}|^2. \tag{18}$$

Average energies of heavy-flavor neutrinos are sufficiently high that odd-parity transitions generated by first-forbidden operators — those proportional either to the momentum/energy transfer or to nucleon velocities — must be considered. In the case of the simplest nucleus under study, ^{9}Be, the charged and neutral current responses were evaluated by including the full momentum transfer dependence of the weak interaction operators, following Refs. [39,40], and summing to all $0\hbar\omega$ and $1\hbar\omega$ final states. The $1\hbar\omega$ shell model space is formed from the one-particle-one-hole excitations of the form $1p(1s)^{-1}$ and $2s1d(1p)^{-1}$; the corresponding cross shell interactions are the Serber-Yukawa force and the Millener-Kurath interaction [41]. As the Slater determinants are formed from harmonic oscillator basis states, the calculation is complete for all first-forbidden operators, which is our main concern. While high multipolarity operators are also included in the calculation, the space of final states is not complete for these. Nor are these operators significant numerically.

As the analogous shell model spaces for the heavier nuclei of interest become somewhat unwieldy, in these cases we estimate the first forbidden response in the Goldhaber-Teller model [42]. This model satisfies the Thomas-Reiche-Kuhn (TRK) sum rule for the E1 response as well as its generalization for L=1 axial responses. That is, the full supermultiplet of giant resonances is described. Transition strengths are carried by doorway states placed in the center of the giant resonance region, which we identify with the E1 photoabsorption peak for neutral current reactions. Note that the model as implemented here assumes N=Z, which is clearly not the case for ^{208}Pb. However the underlying TRK sum rule is proportional to $NZ/A = (A/4)\{1 - [(N - Z)/A]^2\}$. Therefore, even for ^{208}Pb the total strength prediction, $NZ/A \sim A/4$ is good to 5%. Recently continuum RPA calculations of first-forbidden neutrino responses were compared to Goldhaber-Teller predictions for very neutron rich nuclei [43]. The cross sections agreed to better than 40%. Thus the expected uncertainties in using this approximation are not dissimilar to some of those we encountered in our discussions of the allowed responses.

For ^{23}Na and ^{35}Cl, the giant resonance excitation energies, relative to the parent ground states, were taken to be 19 and 20 MeV, respectively, for both charged and neutral current excitations. These values are consistent with the observed E1 photoabsorption peaks. For

neutral current excitations in Pb, we again use the E1 photopeak, 14 MeV, to fix the excitation energy. For ^{208}Pb(ν_e, e^-), the centroid of the spin L=1 strength seen in (p,n) scattering lies about 6.5 MeV above the isobaric analog state in ^{208}Bi, corresponding to an excitation energy of 24.1 MeV relative the ground state of ^{208}Pb. Thus we adopt this as the excitation energy. The strongest first-forbidden contributions to neutrino reactions are spin modes (0^-,1^-, and 2^-).

We do not use the Goldhaber-Teller model to estimate the ^{208}Pb$(\bar{\nu}_e, e^+)$ cross section because, in this direction, the first-forbidden response in largely blocked: only the $1h_{11/2}(p) \rightarrow 1i_{11/2}(n)$ transition is allowed in the naive shell model. The N $\sim$ Z assumption thus cannot be used. However, while we provide no estimate of the cross section, the almost complete blocking of both the allowed and first-forbidden response combined with the Coulomb suppression of positron emission should make this cross section quite small.

The total inelastic cross sections are summarized in Table 1. Results are shown for ten representative neutrino spectra and for all of the relevant interactions, so that any oscillation scenario can be explored. The first four, in the absence of oscillations, would be appropriate for heavy flavor neutrinos, and we believe the differences in these spectra are representative of plausible spectral uncertainties. The first three of these have $\eta_{eff} = 0$, motivated by the Wilson and Mayle calculations, with a range of average energies of 30, 25, and 20 MeV. That is, while 25 MeV might be a best guess for the heavy flavor neutrino mean energy, we want to consider the consequences of a $\pm$ 20% uncertainty in average neutrino energy, which we think in not unreasonable given supernova modeling uncertainties. The fourth case corresponds to a 25 MeV average energy, but has $\eta_{eff} = 3.0$, producing a shape more similar to the numerical spectrum of Janka. The last six spectra all have $\eta = 3.0$; the first three of these correspond to average neutrino energies of 19.2, 16, and 12.8 MeV, and thus are typical of supernova $\bar{\nu}_e$'s, assuming a 20% uncertainty around a best value of 16 MeV. Similarly, the last three spectra, with averages energies of 13.2, 11, and 8.8 MeV, are typical of the ν_e's.

There are some generic features of the cross sections for light nuclei in Table 1. As one would expect, the charged and neutral current cross sections are dominated by allowed transitions for lower neutrino temperatures, with the forbidden contributions becoming increasingly important as the temperature rises. For the most energetic spectra, these two contributions are comparable. Furthermore, for the highest energies which are typical of heavy flavor neutrinos, the ratio of the charged current cross section to the neutral current cross sections (per flavor) is in the range of 3 to 5. Neither of these observations is particularly welcomed from the experimental viewpoint. The presence of an appreciable forbidden contribution enhances the sensitivity of the spectrum-averaged cross section to the particular shape of the distribution. Crudely speaking, the forbidden cross sections contain two extra powers of the neutrino energy. Therefore it appears that, in the absence of an independent measurement of the shape of the energy distribution of the heavy neutrino spectrum, plausible spectral uncertainties could change rate predictions by a factor of three or more. The charged to neutral current cross section ratio is unfortunate because it suggests that the electron and heavy flavor neutrinos would make, in the most favorable case of a hot ν_e spectrum following an oscillation, comparable contributions to total counting rates. In this case there would be no strong flavor sensitivity. For example, making the assumption of the same luminosity per flavor, a $\nu_e \rightarrow \nu_\tau$ oscillation would result in an overall increase in the

rate of inelastic neutrino scattering events by a factor of ~ 1.8 in the case of ^{23}Na, taking ν_e, $\bar{\nu}_e$, and heavy flavor average energies of 11, 16, and 25 MeV, and assuming $\eta_{eff} = 0.0$ for the heavy flavor spectrum. Furthermore we will soon see that most of this enhancement provides no neutrons and is thus not detectable. Thus the rate change is comparable to the (probably optimistic) estimates we made above of cross section uncertainties ($\pm$ 50%), and is dwarfed by the factor-of-several uncertainties associated with plausible spectrum variations. While our main discussion of these issues is deferred to the next section, it is already clear that tricks will be needed to extract oscillation signals from neutron spallation yields.

The ^{208}Pb cross sections require separate discussion, given that estimates have already been made by Hargrove [3]. His allowed neutral current cross section is about a factor of six larger than ours; a factor of about 1.5 of this appears attributable to his somewhat less detailed treatment of the M1 strength profile. The remainder of the discrepancy may be a mistake in the normalization of his β strength function, which appears to lack the factor of 2 found in Eq. (4). (Hargrove also placed all of his strength above the neutron threshold, while we noted that in excess of 55% of the isovector response is to bound states. Thus our allowed cross sections for neutron emission differ by more than an order of magnitude.) However Hargrove did not include first-forbidden contributions, which we find dominate the cross sections for all but the least energetic spectra. For example, our $\eta_{eff} = 0$, $\langle E \rangle = 25$ MeV cross section is 4.55×10^{-40}cm^2, 89% of which comes from first forbidden contributions. The importance of first forbidden contributions in ^{208}Pb is not surprising given the dependence of the Thomas-Reiche-Kuhn sum rule on N and Z, $\sim$ NZ/A $\sim$ A/4, and the lower energy of the ^{208}Pb dipole peak. This total cross section can be compared to that of Hargrove, 3.13 $\times 10^{-40}$ cm^2. The end results are not too different, even though most of our cross section is generated by first forbidden operators not previously considered.

The first-forbidden contributions to charged current cross sections are also very important, about twice the allowed contribution for $\langle E \rangle \sim 25$ MeV. Their influence for lower temperatures is not as great because of the substantially threshold for excited S=1 L=1 giant resonances. Making the same comparison as above to Hargrove, we find our allowed cross sections for $\eta = 0.0$ and $\langle E \rangle = 25$ MeV are in excellent agreement, 20.3 vs 21.9 in units of 10^{-40} cm^2. But our total cross section is substantial larger, 58.0, due to the giant resonance contributions. These differences become particularly interesting when we examine the corresponding spallation cross sections.

The last issue is the probability for producing a signal of one or more spalled neutrons. In the case of the lighter nuclei, unbound states reached by neutrino interactions frequently decay by competing n, p, or alpha channels. We have estimated the neutron emission portion of this cross section by doing Hauser-Feshbach calculations of the decay probabilities as a function of nuclear excitation energy, folding these with the various neutrino cross sections $\sigma(E_\nu)$ corresponding to the total cross sections in Table I. The resulting neutron emission probabilities are given in Table II. Our Hauser-Feshbach calculations are reasonably simple in that they employ a nuclear density-of-states formula that is independent of spin and parity and optical potentials of the Wood-Saxon type without spin-orbit interactions. No attempt is made to estimate direct reaction contributions. Our treatment is identical to that used by Woosley et al. and employs the same code and optical model parameterization [44]. One combines the neutron emission probabilities in Table II with the cross sections in Table I to obtain the needed spectrum- averaged neutron spallation cross sections.

The case of ^{208}Pb is simpler because the enormous Coulomb barrier strongly suppresses charged particle emission. In the case of neutral current excitations, the M1 strength is concentrated in a resonance straddling the neutron emission threshold of 7.37 MeV, as described previously. The neutron resonance measurements of Ref. [36] show that neutron emission dominates over gamma decay even immediately above threshold. Thus the allowed contribution to single neutron emission can be calculated by integrating the cross section over the continuum. The first forbidden cross section was estimated in the Goldhaber-Teller model, with the doorway state placed at the peak of the photoabsorption giant dipole response at ~ 14 MeV. This again straddles an important threshold, as two-neutron emission can occur above 14.1 MeV.

The systematics of two-neutron vs. single neutron emission are well studied. For heavy nuclei there is a surprisingly sharp transition between these two channels occurring typically 2.2 MeV above the two-neutron threshold [45]. As this transition is sharp compared to the breadth of the photoabsorption peak, which has a full width at half maximum $\Gamma \sim 4.3$ MeV [46], it is a very reasonable approximation to associate transitions below 16.3 MeV with single neutron emission, and transitions above this energy with two neutron emission.

The emission probabilities in Table II were calculated by smearing the Goldhaber-Teller results over doorway states distributed according to the measured photoabsorption peak, described as a Gaussian with the above value of Γ. We find that neutral current excitations almost always lead to single neutron emission. The two neutron emission contributions do not exceed 3%. The result that neutral current reactions produce very few multiple neutron events is rather insensitive to the precise description of the photopeak. For example, if the width is increased by a factor of two, the two-neutron emission probability still remains below 10%.

We will argue that this conclusion - that neutral currents effects can be filtered out by observing multiple neutron events - is quite important for oscillation searches. It depends on an assumption, that the spin dipole resonances are located at about the same place as the photoabsorption giant dipole resonance.

Spallation following the charged current reaction $^{208}\mathrm{Pb}(\nu_e, e^-)^{208}\mathrm{Bi}$ differs in an important way. Transitions to states above 6.89 MeV in ^{208}Bi can emit a neutron, above 14.98 MeV can emit two neutrons, and above 22.02 MeV can emit three. The peak of the Gamow-Teller distribution is at 15.5 MeV. Thus a small fraction ($\sim 10\%$) of the allowed charged current cross section can produce multiple neutrons. However the L=1 strength, which dominates the heavy flavor neutrino cross section, is centered at ~ 21.7 MeV, far above the two neutron threshold, and thus always produces multiple neutrons.

Table II gives the resulting neutron emission probabilities. In these calculations, we again attribute all transitions to states above 17.2 MeV in ^{208}Bi (i.e., 2.2 MeV or more above the two-neutron threshold) to multiple-neutron decay. While the single proton emission channel is also open, the Coulomb barrier provides large suppression. Our Hauser-Feshbach calculations yield a very small ratio of of single proton to single neutron emission throughout the excitation energy region spanned by the Gamow-Teller and spin-flip giant resonance peaks.

We repeat for Pb the calculation performed earlier for ^{35}Cl. That is, we evaluate rates with and without a $\nu_e \leftrightarrow \nu_\tau$ oscillation for the canonical temperatures in Table I and under the assumption of a fixed luminosity per flavor, considering all spallation events. One finds

that oscillations increase the rate for all neutron producing events by a factor of $\sim$ 4, which is comparable to the effects of a $\pm$ 20% change in the heavy neutrino spectrum temperature. This is an interesting change, but perhaps not enough to convince skeptics that the ν_τ has a mass. The situation is improved relative to ^{35}Cl because the enhanced charged current cross sections for this high Z target yield a favorable ratio of charged to neutral current cross sections. Thus the change in the charged current rate due to oscillations, a huge factor of ~ 36, is discernible despite neutral current contributions from all other flavors.

But we now see that the situation can be made much, much better. The neutral current signal can be all but turned off by counting only multiple neutron events, while the charged current contribution after oscillations is only modestly reduced. That is, the definitive signal of $\nu_e \leftrightarrow \nu_\tau$ oscillations in a ^{208}Pb detector is a dramatic enhancement in multiple neutron events. A repetition of the calculation above for multiple neutron events yields a ratio of multineutron events with oscillations to those without of ~ 40. In the next section we turn to a more quantitative exploration of this and other strategies for detecting oscillations.

III. STRATEGIES FOR DETECTING FLAVOR OSCILLATIONS: RESULTS AND CONCLUSIONS

In this section we will discuss event rates and possible strategies for LAND, OMNIS, and similar neutron spallation supernova neutrino observatories. The calculations presented in the previous section were performed for specific isotopes of the materials that have been proposed for these targets. For example, ^{208}Pb comprises slightly more than half of natural lead, while ^{35}Cl and ^{23}Na comprise 75% and 100% of natural chlorine and sodium, respectively. (One of the proposed target material in OMNIS in salt.) Therefore a simplification we make is to treat these target materials as being composed of the principal isotopes. Given that we are concerned with neutrino spectrum uncertainties that can change rates by factors of ~ 3, more detailed modeling is difficult to justify. In the case of Pb, the responses are governed by sum rules proportional to N-Z or NZ/A, quantities that vary little from A=208 to A=206, for example. For chlorine one anticipates that our charged current allowed cross sections will be a bit low, given that the ignored isotope ^{37}Cl has N-Z=3 and is more neutron rich than ^{35}Cl.

Interest has been expressed in ^{9}Be because its neutron emission thresholds are so low [47]. In some sense it can be viewed as a neutron target. Its inclusion is also interesting as a theory benchmark, since full shell model calculations satisfying both the allowed and first-forbidden sum rules could be performed. There is general consistency among the first-forbidden responses in Table I for ^{9}Be, ^{23}Na, and ^{35}Cl, even though the last two were evaluated in the somewhat schematic Goldhaber-Teller model.

Because of urgent issues such as a cosmologically interesting muon and/or tauon neutrino mass, proposed supernova neutrino observatories have as their goal the observation of at least the entire galaxy. Thus a typical horizon for such detectors is on the order of the galactic radius, ~ 10 kpc. We begin by expressing the neutrino fluence at earth normed to such a galactic distance. The total number fluence of a given neutrino species (e.g., ν_e, $\bar{\nu}_e$, ν_μ, etc.) is

$$\Phi_\nu \approx 2.67 \times 10^{12} \mathrm{cm}^{-2} \left(\frac{E_{\mathrm{explosion}}}{3 \times 10^{53} \mathrm{ergs}} \right) \left(\frac{\mathrm{MeV}}{\langle E_\nu \rangle} \right) \frac{1}{r^2_{10\,\mathrm{kpc}}}. \tag{19}$$

assuming a total energy in neutrinos of 3 $\times 10^{53}$ ergs, and an equipartition of energy among the six neutrino species, results consistent with most transport calculations (see, e.g., Ref. [27]). The exact distribution of energy among the neutrino species will be an additional source of error, but considerably smaller then that associated with the uncertain spectral distribution. The distance to the supernova, $r_{10\,\mathrm{kpc}}$, is given here in units of 10 kiloparsecs. As a consequence of the equipartition of energy, a neutrino species characterized by a lower average energy will have a higher fluence than one with higher average energy. All of our detector event totals will be calculated with this standard fluence; results for other distances and total explosion energies can be obtained by appropriately scaling to Eq. 19.

In Table III we present the resulting neutron (and multiple neutron Pb) supernova events, summed over flavor, for one-tonne Pb, NaCl, and Be targets, given our assumed normalized neutrino fluence of Eq. 19 for a standard distance of 10 kpc. In the case of neutral current interactions, total inelastic cross sections of these targets (that is, summed over all subsequent decay channels) are not very different when quoted per target mass (or per nucleon): values are within a factor of two of 1.2 $\times 10^{-42}$ cm^2 per nucleon for $E_\nu \sim 25$ MeV.

This is consistent with naive expectations. The forbidden contributions are significant and scale, according to the Thomas-Reiche-Kuhn sum rule, approximately as A. Targets are distinguished, however, by the ease with which they emit neutrons. In the case of ^{35}Cl and ^{23}Na, the greater phase space for proton emission tends to dominate over Coulomb effects, leading to neutral current neutron spallation probabilities of only $\sim 10\%$. But ^{208}Pb and ^{9}Be are more favorable cases, the former because of inhibiting Coulomb barriers and the latter because of an exceptionally low threshold for neutron emission. Thus neutron emission is the dominant decay channel for Pb and Be, producing about an order of magnitude more signal than in a salt detector of equal mass.

While the neutron yield is important in efforts to constrain neutrino masses kinematically, flavor specificity may be more crucial in $\nu_e - \nu_\tau$ oscillation tests. That is, does an anomalously hot ν_e spectrum produce a distinctive signal in a detector? A salt detector, unfortunately, remains problematic. Such an oscillation raises the charged current cross section from an insignificant level to a value comparable to the neutral current cross section summed over flavors. But the (ν_e, e^-) reaction moves one to the proton-rich side of the parent nucleus, yielding neutron spallation probabilities of at most a few percent. The net result is that the oscillation-induced change in total neutron events is quite modest, and would be obscured by existing uncertainties in heavy flavor spectra. To illustrate this point, in Figure 1 we plot neutron events with and without oscillations. In each case there is a band of values corresponding to the range of spectrum choices used in Tables I and II, reflecting existing uncertainties in our knowledge of the neutrino spectra. As the bands, with and without oscillations, overlap substantially, it is clear that neutrino spectral uncertainties will obscure plausible oscillation-induced enhancements of the charged current events.

The ^{9}Be case is somewhat different. The neutron yields following (ν_e, e^-) are exceptionally small, regardless of oscillations. The reaction $(\bar{\nu}_e, e^+)$ has a small cross section but a high neutron yield per reaction; but even in the event of antineutrino oscillations, the effect on the total yield (neutral and charged, summed over flavor) is about 10%. Thus ^{9}Be is a relatively clean neutral current detector.

This property of a ^{9}Be target suggests the possibility of reducing spectral uncertainties by comparing ratios of rates for different nuclear targets. Given that ^{9}Be measures the

neutral current response and has perhaps the most easily calculable cross section, it can be considered a monitor of the heavy flavor temperature: the neutral current rate is not altered by oscillations. Thus, by comparing the event rate in a target with a strong charged current response to that of ^{9}Be, one might hope to remove much of the uncertainty associated with unknown aspects of the ν_τ and ν_μ spectra. Studies of ratios of events might also prove helpful if the distance to the supernova were not known. Superficially this sounds quite attractive as the heavy flavor spectrum also determines the enhanced charged current response following oscillations.

To address this issue more quantitatively, we calculated the ratio of the NaCl events to Be events with and without oscillations. All neutron-producing channels are included, and the heavy flavor, ν_e, and $\bar{\nu}_e$ spectra are allowed to vary over the ranges in Tables I and II. The resulting ranges for the ratios, which are narrower than those of Figure 1, are shown in Figure 2. While this strategy clearly has helped in reducing sensitivity to variation in the spectra, there remain additional uncertainties that affect the ratio, particularly cross section uncertainties. The extended cross section error bars shown in Figure 2 result from combining a $\pm$ 50% uncertainty in the cross section for each target material (Be and NaCl). We regard such an uncertainty as an optimistic guess for what might be achievable, given additional work. It appears to us that a definitive claim of oscillations would be difficult to make in a salt detector, even given a normalizing target such as ^{9}Be.

The situation is much improved for a Pb detector. The first effect apparent from Table I is the exceptionally strong (ν_e, e^-) cross section, a result primarily of the Coulomb enhancement of the cross section. As a result, transmutation of ν_τ's to ν_e's would increase the number of neutron events by a factor of four, as mentioned previously. Thus the comparisons in Figures 1 and 2 are much more favorable. Even more exciting, of course, in the flavor specificity provided by multiple neutron events. The results for multiple neutron events are shown separately in Figures 1 and 2. The enhancement resulting from a complete conversion of ν_τ's to ν_e's is so large, a factor of 40, that it could not be attributed to spectral uncertainties.

We conclude that the ability to identify multiple neutron events with high efficiency in a Pb detector could be of great importance. Perhaps the most important nuclear structure assumption in the Pb calculations is the placement of the spin-flip dipole strength for neutral current excitation at the position of the measured E1 resonance: this leads to the weak neutral current production of multiple neutrons. Presumably the location of the dipole spin-flip strength could checked by spin transfer (p,p') measurements. If this strength were located substantially above the E1 giant resonance, our conclusions would have to be reexamined.

These arguments for finding a signature for neutrino flavor transformation have been based on the assumption that the energy spectrum for one type of neutrino species (the electron neutrino) is completely transformed into that of another (the mu or tau neutrino); i.e., that neutrino flavor evolution through resonances is adiabatic over a broad range of neutrino energies that includes high energies. For the MSW mechanism this will only occur if the density gradient is sufficiently small in the resonance regions, where the transformation takes place. Ignoring neutrino background effects (that is, ignoring neutrino-neutrino neutral current forward exchange scattering contributions to the neutrino effective mass [48,49]), this condition on the vacuum mixing angle for adiabatic evolution may be expressed as [6],

$$\sin^2 2\theta \gtrsim \frac{4\pi E_\nu}{\delta m^2 H} \approx 6\times 10^{-2}\left(\frac{E_\nu}{25\,\mathrm{MeV}}\right)\left(\frac{1\,\mathrm{eV}^2}{\delta m^2}\right)\left(\frac{1\,\mathrm{km}}{H}\right), \tag{20}$$

where $H \approx |\frac{1}{\rho}\frac{d\rho}{dr}|^{-1}$ is the density scale height at the resonance position. Here ρ is the matter density of material at the resonance position. Again, this expression for H ignores neutrino background effects. The magnitude of the neutrino-neutrino forward scattering effects is discussed in Ref.s [48,49]. For a neutrino energy E_ν and mixing parameters δm^2 and $\sin^2 2\theta$ the resonance density is

$$(\rho Y_e)_{\mathrm{res}} \approx 2.6\times 10^5\,\mathrm{g\,cm^{-3}}\left(\frac{\delta m^2}{1\,\mathrm{eV}^2}\right)\left(\frac{25\,\mathrm{MeV}}{E_\nu}\right)\cos 2\theta, \tag{21}$$

where Y_e is the electron fraction. The relevant densities in the supernova range from $\rho \approx 10^{12}\,\mathrm{g\,cm^{-3}}$ at the surface of the the neutron star to $\rho \approx 10\,\mathrm{g\,cm^{-3}}$ in the hydrogen envelope. Therefore, for small mixing angle, flavor transformation can occur for a range of δm^2 of $10^6\mathrm{eV}^2$ to $10^{-5}\mathrm{eV}^2$. The most stringent condition on the mixing angle comes from the outer edges of the supernova. Taking densities from Woosley et al. [44], at this location we find a condition on the mixing angle of $\sin^2 2\theta \gtrsim 10^{-2}$, from Eq. (25). For higher densities, the adiabatic condition gives a less stringent limit.

This range of masses and mixings that would be observable in a supernova includes the popular small-angle MSW solution to the solar neutrino problem. This solution has a mass squared difference, $\delta m^2 \sim 10^{-5}\mathrm{eV}^2$, see for example [50], and can occur either through transformation between $\nu_e \leftrightarrow \nu_\tau$, $\nu_e \leftrightarrow \nu_\mu$ or between $\nu_e \leftrightarrow \nu_s$. In the first case, a similar crossing would occur in the supernova at a similar density, $\rho \approx 100 - 10\,\mathrm{g\,cm^{-3}}$. If on the other hand, if this transformation occurs by $\nu_e \leftrightarrow \nu_\mu$, then the seesaw mechanism would predict a ν_τ mass of 2 - 100 eV [6]. This would necessitate a $\nu_e \leftrightarrow \nu_\tau$ level crossing at high density $\rho \sim 2.6\times 10^5\,(\delta m^2/1\,\mathrm{eV}^2)\,(25\,\mathrm{MeV}/E_\nu)\,\mathrm{g\,cm^{-3}}$, or around $\rho \approx 10^7\mathrm{g\,cm^{-3}}$. There is then an additional $\nu_e \leftrightarrow \nu_\mu$ crossing at lower density, given a standard mass hierarchy. Although this latter scenario presents a more complicated picture of the neutrino transformations occurring in the supernova, the effect in terms of neutron count rates seen in the detector is exactly the same. Therefore, either of these proposed MSW solutions to the solar neutrino problem would imply the presence of matter enhanced neutrino oscillations in the post-core-bounce supernova. Finding a signature of matter enhanced neutrino oscillations in a supernova neutrino detector would provide a completely independent check of this solar solution. And if the solar neutrino problem proved to have some other origin, the wider range of mass differences and mixing angles accessible to supernova neutrino experiments keeps possibilities open for new physics to emerge there.

Finally, we should stress that our primary focus in this paper has been on a specific issue, that of finding a signal for flavor oscillations, including those of the ν_τ. The selection of one target material over another would have to take into account many other issues, e.g., their comparative utility in testing the spreading of neutrino arrival times due to kinematic effects of neutrino masses. Target materials will vary in cost, in ease of neutron detection, and in ambient backgrounds. Our efforts have been directed toward improved event rate estimates and questions of flavor specificity, in the hope that this information will help experimentalists make optimal choices.

This work was supported in part by the National Science Foundation (GF) and the US Department of Energy (GM,WH).

REFERENCES

[1] D. B. Cline *et. al.* , Astrophysical Letters and Communications, **27**, 403, 1990.

[2] D. B. Cline *et. al.* , Phys. Rev. D **50**, 720 (1994), P. F. Smith, Astroparticle Physics, **8** 27 (1997).

[3] C. K. Hargrove *et. al.* , Astroparticle Physics, **5**, 183 (1996).

[4] B. Balantekin, Proceedings of the Jorge Andre Swieca Summer School, Campos de Jordao, Sao Paulo, in press, (1997).

[5] C. S. Lim and W. J. Marciano, Phys. Rev. D. **37**, 1368 (1988); E. Akhmedov, Phys. Lett. **213**, 64 (1988).

[6] S. P. Mikheyev and A. Yu. Smirnov, Sov. J. Nucl. Phys. **24**, 913 (1985); H. A. Bethe, Phys Rev. Lett. **56**, 1305 (1986); W. C. Haxton, Phys. Rev. Lett. **57**, 1271 (1986); S. J. Parke, Phys. Rev. Lett. **57**, 1275 (1986).

[7] J. N. Bahcall, Neutrino Astrophysics, (Cambridge University Press, Cambridge 1989); for a recent review see W. C. Haxton, Ann. Rev. Astron. Astrophys. **33**, 459 (1995).

[8] M. Gell-Mann, P. Ramond, and R. Slansky, in Supergravity, Proceedings of the Workshop, Stoney Brook, New York, 1979, edited by P. Van Nieuwenhuizen and D. Z. Freedman (North-Holland, Amsterdam, 1979); T. Yanagida, in Proceedings of the Workshop on Unified Theory and Baryon Number of the Universe, Tsukuba, Japan, 1979, edited by A. Sawada and A. Sugamoto (KEK Report No. 79-18, Tsukuba, Japan, 1979).

[9] K. S. Babu and R. N. Mohapatra, Phys. Rev. Lett. **70**, 2845 (1993); S. A. Bludman, D. C. Kennedy, and P. G. Langacker, Phys. Rev. D **45**, 1810 (1992); S. Dimopoulos, L. J. Hall, and S. Raby, Phys. Rev. D **47**, R3697 (1993).

[10] Y.-Z. Qian *et al.*, Phys. Rev. Lett **71**, 1965 (1993).

[11] G. M. Fuller, R. W. Mayle, B. S. Meyer, and J. R. Wilson, Astrophys. J. **389**, 517 (1992).

[12] C. Athanassopoulus *et al.*, Phys. Rev. Lett. **75**, 2650 (1995); J. E. Hill, Phys Rev. Lett. **75**, 2650 (1995).

[13] J. M. Gaillard, Nucl. Phys. B **51**, 237 (1996).

[14] K. Kodama, Nucl. Phys B. **51**, 232 (1996).

[15] B. Armbruster *et al.*, Nucl. Phys. B **38**, 235 (1995).

[16] T. Kajita, talk presented at Neutrino '98 (Takayama, Japan), to be published.

[17] P. F. Harrison, D. H. Perkins, W. G. Scott, Phys Lett. B **349**, 137 (1995), C. Y. Cardall and G. M. Fuller, Phys. Rev. D**53**, 4421 (1996), G. L. Fogli, E. Lisi, D. Montanino, Phys. Rev D**54**, 2048 (1996), A. Acker and S. Packvasa, Phys. Lett. B **397**, 209 (1997)

[18] R. W. Mayle and J. R. Wilson, unpublished.

[19] T. Totani, Phys. Rev. Lett. **80**, 2039 (1998).

[20] M. Takita, in *Frontiers of Neutrino Astrophysics*, ed. Y. Suzuki and K. Nakamura (Univ. Acad. Press, Tokyo), p. 135.

[21] A. Burrows, D. Klein, and R. Gandhi, Phys. Rev. D **45**, 3361 (1992).

[22] G. T. Ewan et al., Queen's Univ. Report SNO-87-12 (1987); SNO collaboration, Hyperfine Interactions **130**, 199 (1996).

[23] W. C. Haxton, Phys. Rev. D **36**, 2283 (1987); Y.-Z. Qian and G. M. Fuller, Phys. Rev. D **49**, 1762 (1994).

[24] H. Minakata, private communication.

[25] K. Langanke, P. Vogel, and E. Kolbe, Phys. Rev. Lett. **76**, 2629 (1997).

[26] J. F. Beacom and P. Vogel, Phys .Rev. D58 (1998), J. F. Beacom, P. Vogel, Phys. Rev. D, submitted (1998).
[27] D. S. Miller, J. R. Wilson, and R. W. Mayle, Astrophys. J., **415**, 278 (1993).
[28] H.-T. Janka and W. Hillebrant, Astron. Astrophys., **224**, 49 (1989).
[29] H. Behrends and J. Janecke, *Numerical Tables for Beta Decay and Electron Capture*, Landolt-Bornstein, vol. 4 (Springer-Verlag, Berlin, 1969).
[30] B. A. Brown and B. H. Wildenthal, Phys. Rev. C **28**, 2397 (1983).
[31] D. J. Horen *et al.*, Phys. Lett., **95B**, 27; C. Gaarde et al., Nucl. Phys. A**369**, 258 (1981).
[32] E. Sugarbaker, talk presented at the Workshop on GT and Neutrino Cross Sections, Univ. Pennsylvania, April, 1993.
[33] S. Cohen and D. Kurath, Nucl. Phys. **73**, 1 (1965).
[34] B. H. Wildenthal, Prog. Part. Nucl. Phys. **11**, 5 (1984).
[35] R. M. Laszewski, R. Alarcon, D. S. Dale, and S. D. Hoblit, Phys. Rev. Lett. **61**, 1710 (1988).
[36] R. Kohler et al., Phys. Rev. C**35**, 1646 (1987).
[37] D. Cha, B. Schwesinger, J. Wambach, and J. Speth, Nucl. Phys. A**430**, 321 (1984).
[38] E. Lipparini and A. Richter, Phys. Lett. **144**B, 13 (1984).
[39] T. W. Donnelly and W. C. Haxton, Atomic Data and Nuclear Tables **23**, 103 (1979).
[40] J. D. Walecka, in *Muon Physics*, ed. V. W. Hughes and C. S. Wu (Academic Press, New York, 1975), Vol. 2, p. 113.
[41] D. J. Millener and D. Kurath, Nucl. Phys. A**255**, 315 (1975).
[42] T. W. Donnelly, J. Dubach, and W. C. Haxton, Nucl. Phys. A**251**, 353 (1975).
[43] Y.-Z. Qian, W. C. Haxton, K. Langanke, and P. Vogel, Phys. Rev. C**55**, 1532 (1997).
[44] S. E. Woosley, R. D. Hoffman, W. C. Haxton, Astrophys. J. **356**, 272, (1990)
[45] K. A. Keller, J. Lange, H. Munzel, and G. Pfennig, *Q Values and Excitation Functions of Nuclear Reactions*, Landolt-Bornstein, vol. 5 (Springer-Verlag, Berlin, 1973).
[46] M. Danos and E. G. Fuller, Ann. Rev. Nucl. Science **15**, 29 (1965).
[47] M. Goldhaber, private communication.
[48] G. M. Fuller, R. W. Mayle, J. R. Wilson, and D. N. Schramm, Astrophys. J. **322**, 795 (1987).
[49] Y.-Z. Qian and G. M. Fuller, Phys. Rev. D**51**, 1479 (1995).
[50] N. Hata and P. Langacker, Phys. Rev. D **56**, 6107 (1997).

FIGURES

FIG. 1. The ranges of expected neutron events given the standard neutrino fluences discussed in the text, corresponding to a supernova at a distance of 10 kpc from earth. The results are taken from the cross sections and spallation probabilities of Tables I and II, summed over both neutral and charge current reactions. Two ranges are given, without (left) and with (right) ν_τ to ν_e flavor transformation (labeled by ft). The detector materials are Be, NaCl, and Pb, with cross sections equated to those of the principal isotopes in each case. A clear signal of oscillations would correspond to a pair of ranges with no overlap. Each range is determined from assumed neutrino spectrum and nuclear physics uncertainties. The neutrino spectra are allowed to range over the ($\langle E\rangle$,η) values in the Tables, corresponding to $\pm$20% uncertainties in the canonical heavy flavor neutrino, $\bar{\nu}_e$, and ν_e average energies of 25, 16, and 11 MeV, respectively. The spectral uncertainties produce the inner error bars shown on each range. These errors have been further extended by $\pm$ 50% to indicate possible nuclear physics uncertainties in our estimated cross sections. Two sets of results are given for ^{208}Pb corresponding to all neutron-producing events and to all multiple (denoted by m) neutron events. Note the wide separation in the Pb multiple neutron case between the bands with and without oscillations.

FIG. 2. As in Figure 1, except that ranges for the ratio of NaCl events to Be events and Pb events to Be events are shown. The normalized Pb results are shown for all neutron events and for multiple neutron events only (labeled by m). The inner error bars correspond to the spectral uncertainties, which are reduced because a ratio has been taken. The outer error bars show the effects of cross section uncertainties, which were taken as $\pm$ 50% for both the numerators (Pb, NaCl) and denominator (Be) in taking the ratio of events.

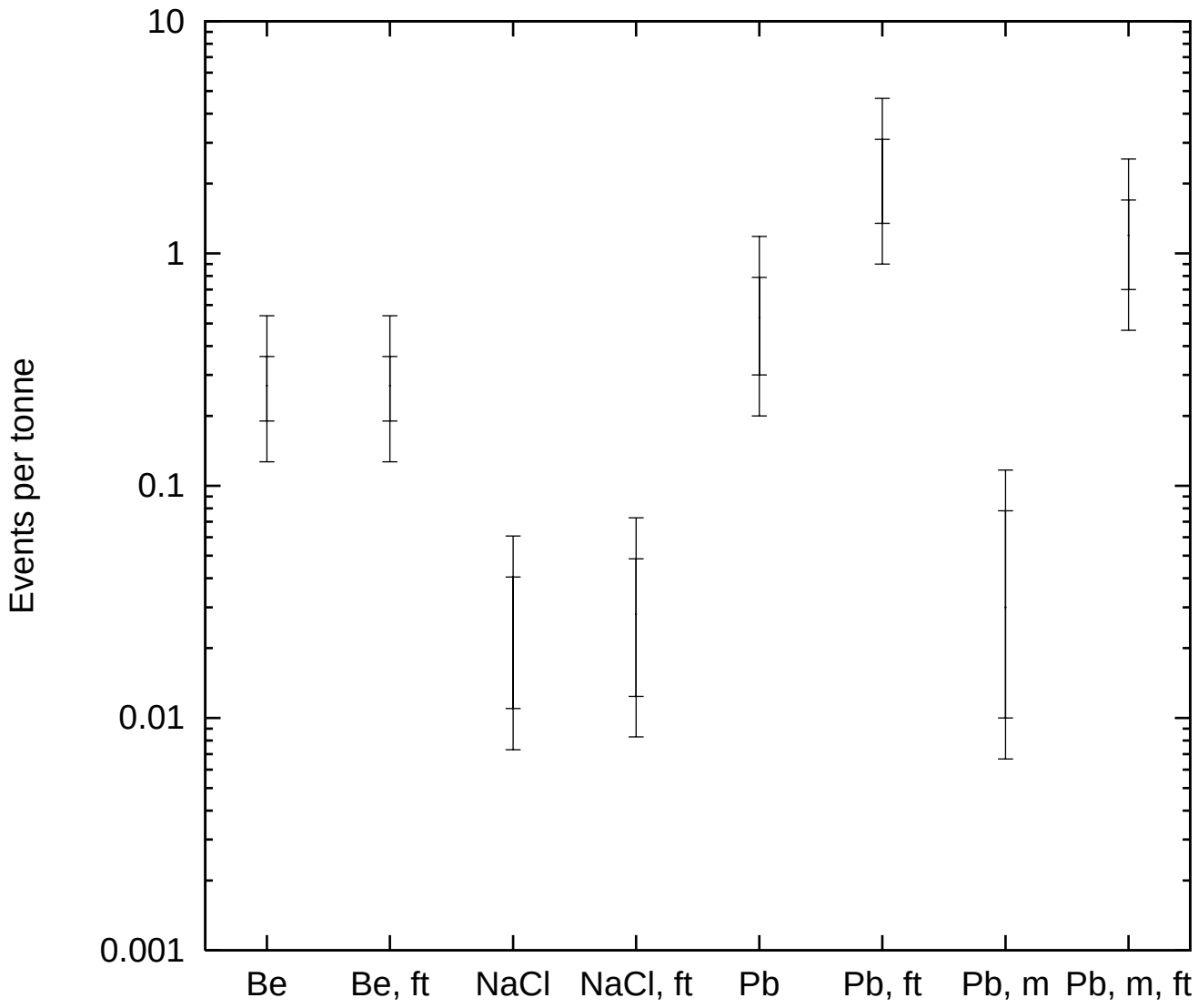
10
1
0.1
0.01
0.001
Events per tonne
Be
Be, ft
NaCl
NaCl, ft
Pb
Pb, ft
Pb, m
Pb, m, ft

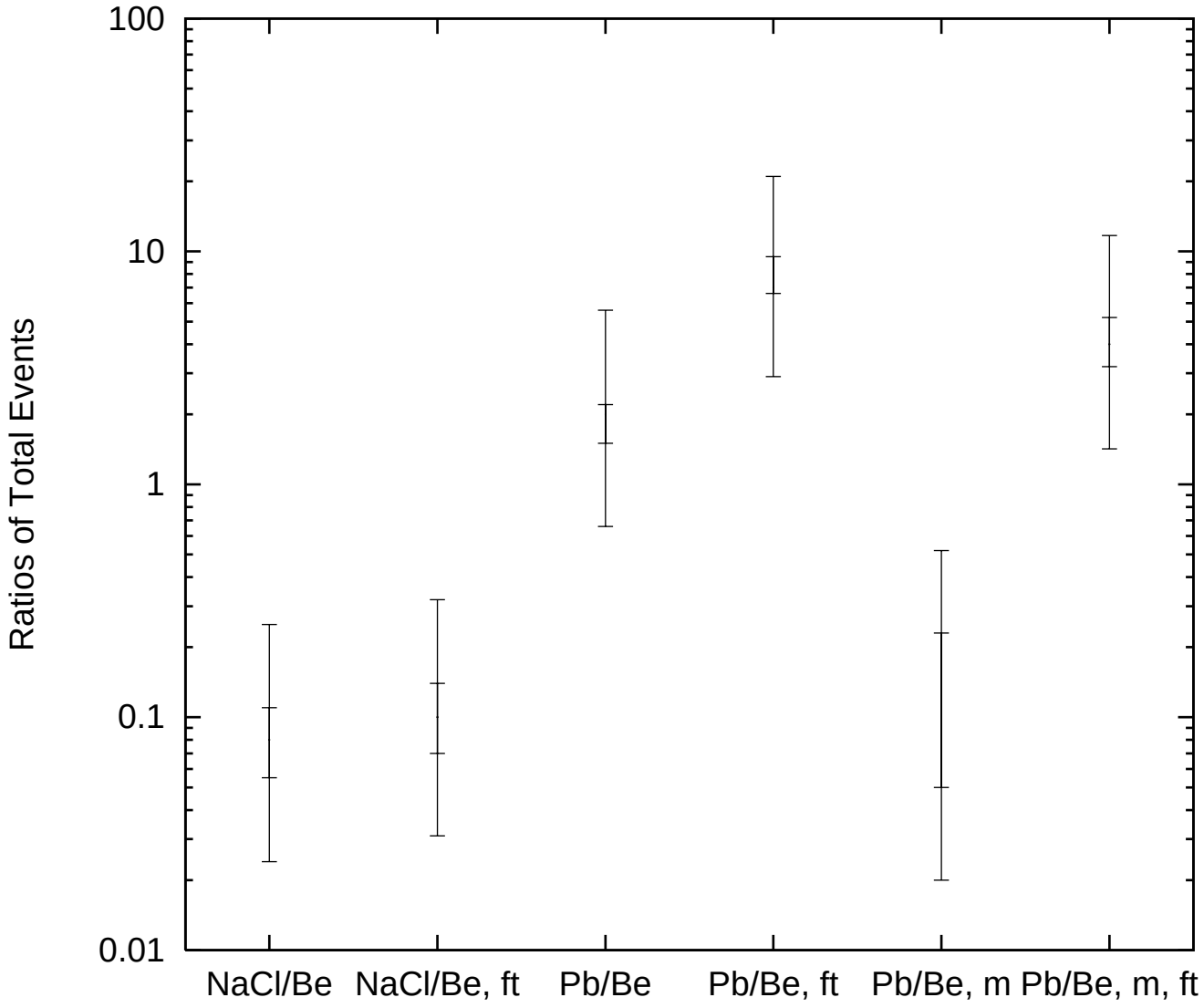
100
10
1
0.1
0.01
Ratios of Total Events
NaCl/Be
NaCl/Be, ft
Pb/Be
Pb/Be, ft
Pb/Be, m
Pb/Be, m, ft

TABLES

TABLE I. Total inelastic neutral current and charge current cross sections for neutrino reactions on ^{208}Pb, ^{35}Cl, ^{23}Na and ^{9}Be, given in units of 10^{-40} cm^2. In each case both allowed and first-forbidden contributions to the cross sections have been calculated. The results correspond to normalized neutrino spectra with a shape defined by the average energy $\langle E\rangle$ and η, as discussed in the text. The first four columns describe a range of heavy flavor neutrino spectra centered around $\langle E\rangle = 25$ MeV; the next three are appropriate for $\bar{\nu}_e$s with $\langle E\rangle \sim 16$ MeV; and the last three correspond to ν_es with $\langle E\rangle \sim 11$. Cross sections are given for each spectrum so that arbitrary oscillation scenarios can be explored.

	E = 30 $\eta = 0$	E = 25 $\eta = 0$	E = 20 $\eta = 0$	E = 25 $\eta = 3$	E = 19.2 $\eta = 3$	E = 16 $\eta = 3$	E = 12.8 $\eta = 3$	E = 13.2 $\eta = 3$	E = 11 $\eta = 3$	E = 8.8 $\eta = 3$
^{208}Pb (ν,ν)										
all	0.810	0.517	0.290	0.453	0.223	0.131	0.0644	0.0714	0.0379	0.0158
for	6.423	4.032	1.996	3.388	1.288	0.527	0.157	0.188	0.0612	0.0125
total	7.233	4.549	2.286	3.841	1.451	0.658	0.221	0.259	0.099	0.028
^{208}Pb $(\bar{\nu},\bar{\nu})$										
all	0.810	0.517	0.290	0.453	0.223	0.131	0.0644	0.0714	0.0379	.0158
for	5.220	3.308	1.664	2.825	1.046	0.457	0.139	0.166	0.055	0.0114
total	6.03	3.825	1.954	3.268	1.272	0.588	0.203	0.237	0.093	0.027
^{208}Pb (ν_e, e^-)										
all	34.22	20.32	10.45	17.28	7.28	3.53	1.202	1.414	0.501	0.107
for	61.92	37.67	17.39	30.22	9.37	3.38	0.736	0.927	0.213	0.024
total	96.14	57.99	27.84	47.50	16.65	6.91	1.938	2.341	0.714	0.131
^{35}Cl (ν,ν)										
all	0.2221	0.1488	0.0863	0.1354	0.0671	0.0389	0.0185	0.0206	0.0107	0.0044
for	0.2155	0.1038	0.0370	0.0643	0.0154	0.0049	0.0010	0.0013	0.0003	0.00004
total	0.4377	0.2527	0.1233	0.1998	0.0825	0.0438	0.0195	0.0219	0.0109	0.0044
^{35}Cl $(\bar{\nu},\bar{\nu})$										
all	0.1820	0.1251	0.0746	0.1162	0.0594	0.0350	0.0170	0.0189	0.0099	0.0042
for	0.1597	0.0792	0.0293	0.0509	0.0127	0.0042	0.0009	0.0011	0.0003	0.00003
total	0.3416	0.2044	0.1039	0.1671	0.0721	0.0392	0.0179	0.0200	0.0102	0.0042
^{35}Cl (ν_e, e^-)										
all	0.6623	0.4229	0.2311	0.3696	0.1695	0.0932	0.0420	0.0471	0.0236	0.0096
for	0.8306	0.3980	0.1411	0.2455	0.0589	0.0189	0.0039	0.0049	0.0011	0.0001
total	1.4929	0.8209	0.3723	0.6152	0.2284	0.1121	0.0459	0.0519	0.0247	0.0098
^{35}Cl $(\bar{\nu}_e, e^+)$										
all	0.0962	0.0683	0.0432	0.0649	0.0364	0.0233	0.0127	0.0139	0.0081	0.0039
for	0.2229	0.1120	0.0423	0.0735	0.0190	0.0064	0.0014	0.0017	0.0004	0.0001
total	0.3191	0.1804	0.0855	0.1383	0.0554	0.0297	0.0141	0.0156	0.0085	0.0040
^{23}Na (ν,ν)										
all	0.2071	0.1401	0.0833	0.1282	0.0663	0.0404	0.0211	0.0232	0.0133	0.0066
for	0.1857	0.0878	0.0309	0.0536	0.0129	0.0042	0.0009	0.0011	0.0003	0.00004

total	0.3928	0.2279	0.1141	0.1818	0.0792	0.0446	0.0220	0.0243	0.0136	0.0066
^{23}Na $(\bar{\nu}, \bar{\nu})$										
all	0.1659	0.1153	0.0706	0.1076	0.0575	0.0357	0.0191	0.0209	0.0122	0.0061
for	0.1353	0.0662	0.0242	0.0421	0.0106	0.0035	0.0008	0.0010	0.0002	0.00003
total	0.3012	0.1815	0.0948	0.1497	0.0681	0.0393	0.0199	0.0218	0.0124	0.0062
^{23}Na (ν_e, e^-)										
all	0.6992	0.4671	0.2739	0.4231	0.2160	0.1306	0.0677	0.0743	0.0423	0.020
for	0.6245	0.2929	0.1022	0.1776	0.0426	0.0139	0.0029	0.0037	0.0009	0.0001
total	1.3237	0.7599	0.3761	0.6007	0.2586	0.1444	0.0706	0.0780	0.0431	0.0205
^{23}Na $(\bar{\nu}_e, e^+)$										
all	0.0772	0.0518	0.0303	0.0474	0.0238	0.0138	0.0066	0.0073	0.0037	0.001
for	0.2140	0.1061	0.0397	0.0689	0.0179	0.0061	0.0014	0.0017	0.0004	0.0001
total	0.2913	0.1580	0.0700	0.1163	0.0417	0.0200	0.0079	0.0090	0.0041	0.0015
^{9}Be (ν, ν)										
all	0.1354	0.0933	0.0574	0.0862	0.0473	0.0305	0.0173	0.0188	0.0116	0.0063
for	0.0964	0.0428	0.0145	0.0250	0.0062	0.0022	0.0006	0.0007	0.0002	0.0001
total	0.2317	0.1362	0.0719	0.1112	0.0535	0.0327	0.0179	0.0195	0.0119	0.0063
^{9}Be $(\bar{\nu}, \bar{\nu})$										
all	0.1053	0.0750	0.0478	0.0709	0.0404	0.0267	0.0155	0.0168	0.0106	0.0058
for	0.0659	0.0309	0.0111	0.0191	0.0050	0.0019	0.0005	0.0006	0.0002	0.0001
total	0.1712	0.1059	0.0589	0.0899	0.0455	0.0285	0.0161	0.0174	0.0108	0.0059
^{9}Be (ν_e, e^-)										
all	0.7233	0.5066	0.3202	0.4723	0.2692	0.1796	0.1077	0.1156	0.0754	0.0442
for	0.3268	0.1465	0.0504	0.0866	0.0222	0.0082	0.0023	0.0027	0.0009	0.0002
total	1.0500	0.6531	0.3707	0.5589	0.2914	0.1877	0.1099	0.1184	0.0763	0.0444
^{9}Be $(\bar{\nu}_e, e^+)$										
all	0.0145	0.0084	0.0040	0.0067	0.0025	0.0011	0.0004	0.0004	0.0001	0.0000
for	0.0715	0.0317	0.0103	0.0180	0.0039	0.0012	0.0002	0.0003	0.0001	0.0000
total	0.0860	0.0401	0.0143	0.0247	0.0064	0.0023	0.0006	0.0007	0.0002	0.0000

TABLE II. Neutron spallation probabilities for allowed, forbidden, and all neutrino induced transitions in Be, Na, Cl, and Pb. The calculations are Hauser-Feshbach type, except in the case of Pb, as discussed in the text. The Pb results are given separately for single and multiple neutron spallation.

E	30	25	20	25	19.2	16	12.8	13.2	11	8.8
η	0	0	0	3	3	3	3	3	3	3
$^{208}\mathrm{Pb}\,(\nu,\nu)$	1n									
allowed	0.443	0.441	0.438	0.440	0.435	0.430	0.422	0.423	0.415	0.403
forbidden	0.969	0.970	0.972	0.972	0.975	0.978	0.982	0.981	0.985	0.992
$^{208}\mathrm{Pb}\,(\bar{\nu},\bar{\nu})$	1n									
allowed	0.443	0.441	0.438	0.440	0.435	0.430	0.422	0.423	0.415	0.403
forbidden	0.969	0.970	0.972	0.972	0.975	0.978	0.982	0.981	0.985	0.992
$^{208}\mathrm{Pb}\,(\nu_e,e^-)$	1n									
allowed	0.904	0.908	0.914	0.912	0.922	0.931	0.942	0.940	0.950	0.962
forbidden	0.0	0.0	0.0	0.0	0.0	0.0	0.0	0.0	0.0	0.0
$^{208}\mathrm{Pb}\,(\nu,\nu)$	2n									
allowed	0.0	0.0	0.0	0.0	0.0	0.0	0.0	0.0	0.0	0.0
forbidden	0.031	0.030	0.028	0.028	0.025	0.022	0.018	0.019	0.015	0.008
$^{208}\mathrm{Pb}\,(\bar{\nu},\bar{\nu})$	2n									
allowed	0.0	0.0	0.0	0.0	0.0	0.0	0.0	0.0	0.0	0.0
forbidden	0.031	0.030	0.028	0.028	0.025	0.022	0.018	0.019	0.015	0.008
$^{208}\mathrm{Pb}\,(\nu_e,e^-)$	2n									
allowed	0.096	0.092	0.086	0.088	0.078	0.069	0.058	0.060	0.050	0.038
forbidden	1. 0	1. 0	1. 0	1. 0	1. 0	1. 0	1. 0	1. 0	1. 0	1. 0
$^{35}\mathrm{Cl}\,(\nu,\nu)$										
allowed	0.0032	0.0029	0.0025	0.0026	0.0021	0.0017	0.0012	0.0012	0.0009	0.0005
forbidden	0.0917	0.0917	0.0917	0.0917	0.0917	0.0917	0.0917	0.0917	0.0917	0.0917
total	0.0468	0.0394	0.0292	0.0313	0.0188	0.0118	0.0058	0.0064	0.0033	0.0012
$^{35}\mathrm{Cl}\,(\bar{\nu},\bar{\nu})$										
allowed	0.0032	0.0029	0.0025	0.0026	0.0021	0.0017	0.0012	0.0012	0.0008	0.0005
forbidden	0.0917	0.0917	0.0917	0.0917	0.0917	0.0917	0.0917	0.0917	0.0917	0.0917
total	0.0446	0.0373	0.0276	0.0298	0.0179	0.0112	0.0056	0.0062	0.0031	0.001
$^{35}\mathrm{Cl}\,(\nu_e,e^-)$										
allowed	0.0013	0.0011	0.0009	0.0010	0.0007	0.0005	0.0003	0.0003	0.0002	0.000
forbidden	0.0152	0.0152	0.0152	0.0152	0.0152	0.0152	0.0152	0.0152	0.0152	0.0152
total	0.0090	0.0079	0.0063	0.0066	0.0044	0.0030	0.0015	0.0017	0.0008	0.0003
$^{35}\mathrm{Cl}\,(\bar{\nu}_e,e^+)$										
allowed	0.4468	0.4346	0.4150	0.4278	0.3988	0.3723	0.3311	0.3374	0.2968	0.2368
forbidden	0.9046	0.9046	0.9046	0.9046	0.9046	0.9046	0.9046	0.9046	0.9046	0.9046
total	0.7666	0.7266	0.6571	0.6810	0.5720	0.4867	0.3867	0.3998	0.3262	0.245
$^{23}\mathrm{Na}\,(\nu,\nu)$										
allowed	0.0478	0.0419	0.0344	0.0375	0.0277	0.0208	0.0131	0.0141	0.0087	0.0040
forbidden	0.3058	0.3058	0.3058	0.3058	0.3058	0.3058	0.3058	0.3058	0.3058	0.3058

total	0.1698	0.1436	0.1078	0.1166	0.0729	0.0476	0.0247	0.0273	0.0144	0.0055
^{23}Na $(\bar{\nu}, \bar{\nu})$										
allowed	0.0487	0.0429	0.0352	0.0386	0.0284	0.0213	0.0133	0.0143	0.0088	0.004
forbidden	0.3058	0.3058	0.3058	0.3058	0.3058	0.3058	0.3058	0.3058	0.3058	0.3058
total	0.1642	0.1388	0.1044	0.1138	0.0716	0.0470	0.0246	0.0271	0.0144	0.005
^{23}Na (ν_e, e^-)										
allowed	0.0041	0.0032	0.0022	0.0025	0.0014	0.0009	0.0004	0.0004	0.0002	0.0001
forbidden	0.0936	0.0936	0.0936	0.0936	0.0936	0.0936	0.0936	0.0936	0.0936	0.0936
total	0.0463	0.0380	0.0271	0.0294	0.0166	0.0098	0.0043	0.0048	0.0021	0.0006
^{23}Na $(\bar{\nu}_e, e^+)$										
allowed	0.3561	0.3449	0.3265	0.3362	0.3075	0.2820	0.2437	0.2495	0.2136	0.1650
forbidden	0.5822	0.5822	0.5822	0.5822	0.5822	0.5822	0.5822	0.5822	0.5822	0.5822
total	0.5222	0.5043	0.4716	0.4819	0.4255	0.3741	0.3019	0.3123	0.2514	0.1810
^{9}Be (ν, ν)										
allowed	0.7360	0.7444	0.7545	0.7500	0.7626	0.7716	0.7826	0.7811	0.7896	0.7990
forbidden	0.5208	0.5191	0.5150	0.5155	0.5071	0.4997	0.4904	0.4916	0.4849	0.4799
total	0.6465	0.6735	0.7063	0.6973	0.7330	0.7531	0.7728	0.7704	0.7835	0.7961
^{9}Be $(\bar{\nu}, \bar{\nu})$										
allowed	0.7350	0.7431	0.7533	0.7482	0.7612	0.7704	0.7816	0.7801	0.7889	0.7984
forbidden	0.5267	0.5245	0.5198	0.5204	0.5117	0.5042	0.4949	0.4961	0.4896	0.4853
total	0.6548	0.6794	0.7093	0.6999	0.7335	0.7530	0.7724	0.7700	0.7831	0.7956
^{9}Be (ν_e, e^-)										
allowed	0.0000	0.0000	0.0000	0.0000	0.0000	0.0000	0.0000	0.0000	0.0000	0.0000
forbidden	0.0068	0.0055	0.0040	0.0040	0.0023	0.0014	0.0007	0.0007	0.0003	0.0001
total	0.0021	0.0012	0.0005	0.0006	0.0002	0.0001	0.0000	0.0000	0.0000	0.0000
^{9}Be $(\bar{\nu}_e, e^+)$										
allowed	0.6599	0.6279	0.5832	0.5932	0.5263	0.4714	0.3943	0.4056	0.3368	0.2481
forbidden	0.9435	0.9560	0.9698	0.9700	0.9831	0.9895	0.9947	0.9942	0.9969	0.9987
total	0.8958	0.8873	0.8618	0.8673	0.8050	0.7367	0.6242	0.6415	0.5323	0.3851

TABLE III. The total number of neutron events for one tonne (10^3 kg) Pb, NaCl, and Be targets, given a neutrino fluence corresponding to 5 $\times 10^{52}$ ergs per neutrino type (ν_e,$\bar{\nu}_e$, etc.), a supernova distance of 10 kpc, and average neutrino energies as shown. Results are shown separately for allowed and forbidden contributions and, in the case of Pb, for single and multiple neutron events.

	$\nu_\mu + \bar{\nu}_\mu + \nu_\tau + \bar{\nu}_\tau$	ν_e	$\bar{\nu}_e$	Total
^{208}Pb				
1 n	0.439	0.038	0.024	0.50
2 n	0.013	0.017	0.0005	0.030
1n, $\nu_e \leftrightarrow \nu_\mu$ or $\nu_e \leftrightarrow \nu_\tau$	0.325	0.684	0.024	1.0
2n, $\nu_e \leftrightarrow \nu_\mu$ or $\nu_e \leftrightarrow \nu_\tau$	0.010	1.20	0.005	1.2
^{35}Cl				
all n	0.0064	2.3×10^{-5}	0.0042	0.011
all n, $\nu_e \leftrightarrow \nu_\mu$ or $\nu_e \leftrightarrow \nu_\tau$	0.0046	0.0030	0.0042	0.012
^{23}Na				
all n	0.0318	1.8×10^{-4}	0.0040	0.036
all n, $\nu_e \leftrightarrow \nu_\mu$ or $\nu_e \leftrightarrow \nu_\tau$	0.0229	0.0169	0.0040	0.044
^{9}Be				
all n	0.229	0.0148	0.026	0.27
all n, $\nu_e \leftrightarrow \nu_\mu$ or $\nu_e \leftrightarrow \nu_\tau$	0.180	0.0648	0.026	0.27